Journal of Thermal Analysis and Calorimetry, Vol. 81 (2005) 603–607

HEAT CAPACITY AND MAGNETIC PHASE TRANSITION OF TWO-DIMENSIONAL METAL-ASSEMBLED COMPLEX $(NEt_4)[\{Mn^{III}(salen)\}_2Fe^{III}(CN)_6]$*

Y. Miyazaki[1]**, *T. Sakakibara*[1], *H. Miyasaka*[2], *N. Matsumoto*[3] *and M. Sorai*[1]

[1]Research Center for Molecular Thermodynamics, Graduate School of Science, Osaka University, Toyonaka, Osaka 560-0043, Japan
[2]Department of Chemistry, Graduate School of Science, Tokyo Metropolitan University, Minami-ohsawa 1-1, Hachioji, Tokyo 192-0397, Japan
[3]Department of Chemistry, Faculty of Science, Kumamoto University, 2-39-1 Kurokami, Kumamoto 860-8555, Japan

Heat capacity measurements of the two-dimensional metal-assembled complex, $(NEt_4)[\{Mn^{III}(salen)\}_2Fe^{III}(CN)_6]$ [Et=ethyl, salen= N,N'-ethylenebis(salicylideneaminato) dianion], were performed in the temperature range between 0.2 and 300 K by adiabatic calorimetry. A ferrimagnetic phase transition was observed at T_{c1}=7.51 K. Furthermore, another small magnetic phase transition appeared at T_{c2}=0.78 K. Above T_{c1}, a heat capacity tail arising from the short-range ordering of the spins characteristic of two-dimensional magnets was found. The magnetic enthalpy and entropy were evaluated to be ΔH=291 J mol^{-1} and ΔS=27.4 J K^{-1} mol^{-1}, respectively. The experimental magnetic entropy agrees roughly with $\Delta S=R\ln(5\cdot5\cdot2)$ (=32.5 J K^{-1} mol^{-1}; R being the gas constant), which is expected for the metal complex with two Mn(III) ions in high-spin state (spin quantum number S=2) and one Fe(III) ion in low-spin state (S=1/2). The heat capacity tail above T_{c1} became small by grinding and pressing the crystal. This mechanochemical effect would be attributed to the increase of lattice defects and imperfections in the crystal lattice, leading not only to formation of the crystal with a different magnetic phase transition temperature but also to decrease of the magnetic heat capacity and thus the magnetic enthalpy and entropy.

Keywords: *heat capacity, magnetic phase transition, mechanochemical effect, metal-assembled complex*

Introduction

Molecule-based magnets have drawn great attention of researchers because they have potentialities to provide a variety of magnetism in comparison to ordinary metals and metal oxides [1–7]. In particular, the so-called 'metal-assembled complexes' can generate more specific spatial, electronic, and magnetic structures than molecule-based magnets consisting of discrete molecules such as pure organic radicals and typical metal complexes. Reaction between hexacyanometalate anions $M(CN)_6^{n-}$ and cationic metal-complex species consisting of a paramagnetic metal center and (an) organic ligand(s) can lead to metal-assembled complexes, the so-called Prussian blue-like system. The merit of this system is that one can control the dimensionality of magnetic lattice (one-, two-, and three-dimensional structures) and tune the magnetic properties by changing the ligand chemical structures. Many Prussian blue-like metal-assembled complexes have so far been synthesized and studied [8–11].

Metal-assembled complex,$(NEt_4^+)[\{Mn^{III}(salen)^{2-}\}_2Fe^{III}(CN^-)_6]$ [Et=ethyl, salen=N,N'-ethylenebis(salicylideneaminato) dianion, Fig. 1a], which is abbreviated as MnFe-sal, has been prepared by reacting $[Mn(salen)(H_2O)]ClO_4$ and $(NEt_4)_3[Fe(CN)_6]$ in a similar procedure to other salen-derivative complexes [8, 9]. This complex comprises two high-spin Mn^{3+} ions (spin quantum number S=2) and one low-spin Fe^{3+} ion (S=1/2) per composition formula unit. X-ray crystallography [12] revealed that the MnFe-sal crystal belongs to the monoclinic crystal system with the space group $P2_1/c$ and forms a two-dimensional network structure by the combination of 2:1 of $[Mn(salen)]^+$ and $[Fe(CN)_6]^{3-}$ as schematically shown in Fig. 1b. Magnetic measurement [12] showed that the MnFe-sal complex possesses an antiferromagnetic interaction through the Fe–CN–Mn bridge and exhibits a ferrimagnetic phase transition at T_c=7.7 K.

In addition to magnetic measurements, adiabatic heat capacity calorimetry is a very powerful tool for investigation of magnetic properties of magnetic materials. This method enables us to obtain not only precise magnetic phase transition temperature, magnetic heat capacity, and entropy gain due to the magnetic origin but also the type of spin-spin interaction, magnetic dimensionality, and the type of magnetism [13–17]. In the present study, we have performed heat

* Contribution No. 97 from the research Centre for Molecular Thermodynamics

** Author for correspondence: miyazaki@chem.sci.osaka-u.ac.jp

1388–6150/$20.00

Akadémiai Kiadó, Budapest, Hungary
Springer, Dordrecht, The Netherlands

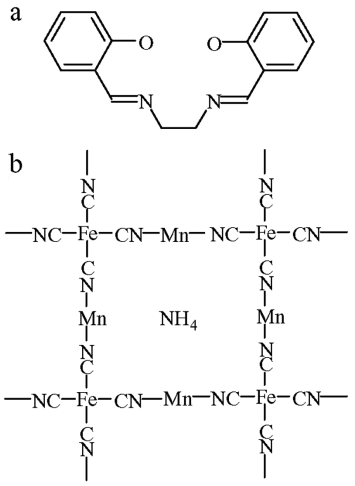

Fig. 1 a – Molecular structure of salen. b – Schematic drawing of two-dimensional assembly of $[Mn(salen)]^+$ and $[Fe(CN)_6]^{3-}$ in the MnFe-sal crystal, where $[Mn(salen)]^+$ is simply expressed by Mn

capacity measurement of the MnFe-sal complex to elucidate its magnetic properties in detail.

Experimental

MnFe-sal polycrystals were synthesized according to the method described elsewhere [12]. Heat capacity measurements of the sample were carried out with two types of adiabatic calorimeters depending on the temperature regions: a very-low-temperature adiabatic calorimeter workable with a $^3He/^4He$ dilution refrigerator (dilution calorimeter) [18] in the 0.2–30 K temperature region and a low-temperature adiabatic calorimeter for small samples (microcalorimeter) [19] in the 7–301 K temperature region. For the microcalorimeter, 0.64160 g of as-grown polycrystalline sample (designated as 'sample A' hereafter) was loaded into a gold-plated copper cell and sealed with indium wire under 0.1 MPa of ^4He gas atmosphere to aid thermal equilibration within the cell. For the dilution calorimeter, the polycrystalline sample was ground and pressed to ca. 1 MPa to form a disc with 2 cm in diameter ('sample B'), and 1.47350 g of the sample was loaded into a gold-plated copper cell with no heat exchange medium. Since the heat capacity data for the samples A and B did not agree well at low temperatures, heat capacity measurements were repeated for 0.54719 g of the sample prepared by crashing the disc used as the sample B ('sample C' hereafter) with the microcalorimeter. Buoyancy correction for the sample mass was made by assuming the density of 1.432 g cm^{-3} calculated by the X-ray crystallographic data [12].

Results and discussion

Figure 2 shows molar heat capacities C_p of the MnFe-sal crystals determined for three different samples A, B, and C *vs.* temperature *T*. For the as-grown sample A, a heat capacity peak due to the ferrimagnetic phase transition was observed at T_{c1}=7.51 K, which is in good agreement with T_c=7.7 K by the magnetic measurement [12]. Above T_{c1}, a large heat capacity tail arising from the short-range ordering of the spin alignment characteristic of low-dimensional magnets was observed. On the other hand, the heat capacities of the pelletted sample B exhibited another magnetic phase transition at T_{c2}=0.78 K in addition to the ferrimagnetic phase transition at almost the same temperature as that of the sample A and the short-range-order effect. Interestingly, the thermal anomaly due to the short-range-order effect for the sample B became a little bit smaller than that for the sample A, namely, the MnFe-sal crystal showed a kind of mechanochemical effect caused by grinding and pressing the crystal. Such a mechanochemical effect was also found in $K[\{Mn^{III}(3\text{-MeOsalen})\}_2Fe^{III}(CN)_6]$ [3-MeOsalen= N,N'-ethylenebis(3-methoxysalicylideneaminato) dianion] (abbreviated as MnFe-mos) crystal [20]. The

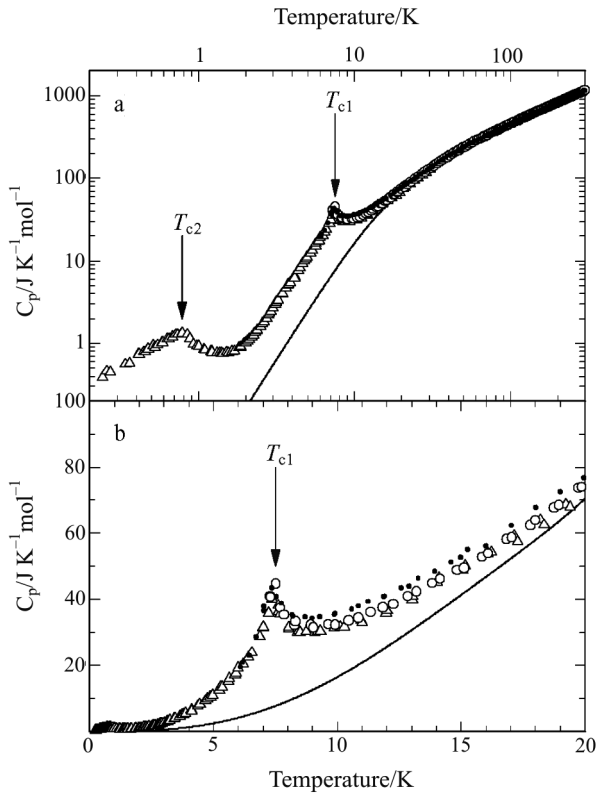

Fig. 2 Molar heat capacities of the MnFe-sal crystals a – in the whole experimental temperature range and b – around the magnetic phase transitions. ○ – sample A, △ – sample B, ● – sample C. Solid curve shows the normal heat capacity for the sample A

remeasured heat capacities of the sample C prepared by crushing the disc sample B were recovered completely (Fig. 2). Slightly large C_p data of the sample C compared with those of the sample A at low temperatures are perhaps ascribed to the tendency that the magnetic properties of the MnFe-sal crystal are very sensitive to even a weak perturbation such as crushing of a sample pellet. Since the present MnFe-sal crystal belongs to a category of soft materials, it easily suffers such a mechanochemical effect.

To separate the magnetic contribution from the whole heat capacity of the MnFe-sal complex, the normal heat capacity was determined as follows. At low temperatures, the heat capacities far above the magnetic phase transition temperature may be approximated by the following equation:

$$C_p=c_3T^3+c_5T^5+c_7T^7+c_{-2}T^{-2} \quad (1)$$

where the first three terms indicate the normal heat capacity and the last term corresponds to the contribution from the short-range-order effect of the spins [21]. We tried to fit the heat capacity data of the sample A alone between 12 and 20 K to Eq. (1), because the sample B has been perturbed by the mechanochemical effect and thus the use of its heat capacities is not appropriate. Moreover, since mild grinding and weak pressing of the sample with 1 MPa would bring about negligibly small change in the lattice vibrations, the normal heat capacity determined from the data of the sample A is applicable to the evaluation of the magnetic heat capacity C_{mag} of the sample B. The derived parameters are $c_3=2.10\cdot10^{-2}$ J K^{-4} mol^{-1}, $c_5=-4.96\cdot10^{-5}$ J K^{-6} mol^{-1}, $c_7=4.79\cdot10^{-8}$ J K^{-8} mol^{-1}, and $c_{-2}=1.79\cdot10^{3}$ J K mol^{-1}. Figure 3 represents the magnetic heat capacities of the samples A and B obtained by subtraction of the normal heat capacities from the total heat capacities. The remarkable heat capacity anomaly above T_{c1} can be regarded as the short-range-order effect for the two-dimensional magnetic system from its shape and the structural analysis [12].

The magnetic enthalpy and entropy acquisitions for the samples A and B were obtained by integrating the magnetic heat capacities with respect to T and ln$T$, respectively. The magnetic heat capacities of the sample A at very low temperatures were regarded as being equal to those of the sample B. The magnetic heat capacity was extrapolated from 0.2 down to 0 K by use of the spin wave theory [13] described later. On the other hand, extrapolation of the magnetic heat capacity up to infinite temperature was made by use of the T^{-2} term in Eq. (1), where the coefficient of the T^{-2} term for the sample B was estimated by fitting the C_{mag} data between 8 and 20 K as being $1.45\cdot10^{3}$ J K mol^{-1} (dashed curve in Fig. 3b). As mentioned above, the MnFe-sal complex exhibited the small magnetic phase transition at T_{c2}=0.78 K besides the main ferrimagnetic phase transition at T_{c1}=7.51 K. If both the magnetic phase transitions are taken into consideration, the experimental magnetic enthalpies and entropies are ΔH=291 J mol^{-1} and ΔS=27.4 J K^{-1} mol^{-1} for the sample A, and ΔH=257 J mol^{-1} and ΔS=25.5 J K^{-1} mol^{-1} for the sample B. On the other hand, if only the main ferrimagnetic phase transition is considered, the experimental magnetic enthalpies and entropies are ΔH=289 J mol^{-1} and ΔS=25.3 J K^{-1} mol^{-1} for the sample A, and ΔH=256 J mol^{-1} and ΔS=23.4 J K^{-1} mol^{-1} for the sample B,

The theoretical magnetic entropy expected for the MnFe-sal complex is $\Delta S=R\ln(5\cdot5\cdot2)$ (=32.5 J K^{-1} mol^{-1}) since there are two Mn^{3+} ions with S=2 and one Fe^{3+} ion with S=1/2 per formula unit in the MnFe-sal complex. The experimental magnetic entropy of the sample A due to the main ferrimagnetic phase transition alone, 25.3 J K^{-1} mol^{-1}, is obviously smaller than the theoretical value. This implies that a part of the MnFe-sal crystals would suffer slight strain and/or deformation which leads to the lowering of the magnetic phase transition temperature, as seen from the fact that the C_p data of the sample B perturbed mechanically during the pellet formation exhibit the

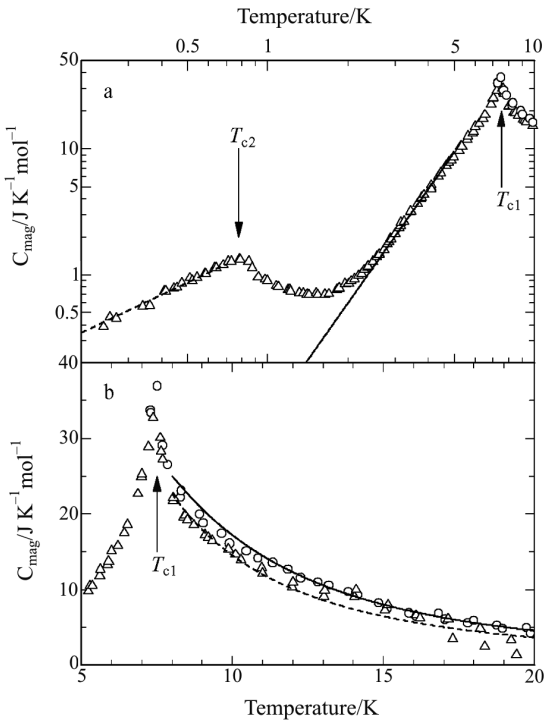

Fig. 3 Magnetic heat capacities of the MnFe-sal crystals. ○ – sample A, △ – sample B. a – Solid and dashed curves indicate the heat capacities derived from the spin wave theory (see the text). b – Solid curve represents the theoretical heat capacity for the S=3/2 two-dimensional ferromagnetic Heisenberg model of square lattice with J/k_B=1.4 K. Dashed curve shows extrapolation up to infinite temperature by T^{-2} term for the samples B

magnetic phase transition at 0.78 K. The experimental magnetic entropy of the sample A including the contribution of both the magnetic phase transitions, 27.4 J K^{-1} mol^{-1}, is also somewhat smaller than the theoretical value. This would be due to the existence of the paramagnetic species which do not undergo magnetic ordering in the experimental temperature region. Ambiguity for the determination of the normal heat capacity would also be the cause. On the other hand, the reduction of the magnetic entropy of the sample B is attributable to the increment of the paramagnetic species characteristic of the high-temperature phase arising from the enhanced lattice defects and imperfections in the crystal lattice produced by the mechanochemical effect, as found in the MnFe-mos complex [20]. It may be possible that a part of the MnFe-sal crystals turned to the crystals containing low-spin Mn^{3+} ions (S=1), which gives rise to the lower theoretical magnetic entropy R ln (3·3·2) (=24.0 J K^{-1} mol^{-1}). However, it is very unlikely that soft grinding and pressing of the sample under a low pressure such as 1 MPa caused such a drastic change from the high- to the low-spin state.

Next, we tried to analyze the magnetic heat capacities of the sample A above T_{c1} on the basis of two-dimensional magnetic models. According to the magnetic study [12], the MnFe-sal complex is ferrimagnetic, that is, it consists of antiferromagnetic layers. Since the present complex has a complicated magnetic system as the MnFe-mos complex does [8, 20], we approximated the actual layer by an S=3/2 two-dimensional Heisenberg system, where S=3/2 is an averaged spin quantum number of two S=2 spins and one S=1/2 spin. The C_{mag} data of the sample A between 11 and 20 K was fitted to three moles of an S=3/2 two-dimensional Heisenberg model of square lattice [22–24]. The best fit was obtained for a rather small value of the ferromagnetic exchange interaction J/k_B=1.4 K (k_B: the Boltzmann constant) as shown by a solid curve in Fig. 3b. The derived J value is close to the value J/k_B=1.6 K in the MnFe-mos complex [20], because of similar compositions and crystal dimensions [8, 12]. The ferromagnetic interaction does not conflict with the bulk antiferromagnetic character [12]. The dominant magnetic interaction in the complex at high temperatures is the intralayer short-range ferromagnetic interaction, while at low temperatures the interlayer long-range antiferromagnetic interaction brings about the three-dimensional magnetic order. Similar case has been encountered in the $Mn^{II}Cu^{II}$(obbz)·$5H_2O$ [25] and $Mn^{II}Cu^{II}$(obbz)·H_2O [26] [obbz=oxamidobis(benzoato)] complexes having one- and two-dimensional ferrimagnetic networks, respectively, where their magnetic heat capacities in the temperature region of the short-range order can be fitted well by use of one-dimensional and two-dimensional ferromagnetic Heisenberg models, respectively. The assumption that the rather complicated actual magnetic system was approximated by a simple square lattice consisting of homogeneous spins seems to cause the low J value in comparison with T_{c1}.

Finally, we shall discuss the magnetic heat capacities at very low temperatures. In general, heat capacities of magnetic substances at very low temperatures follow the spin wave theory [13]:

$$C_{mag} \propto T^{d/n} \tag{2}$$

where d stands for the dimensionality of magnetic lattice and n is defined as the exponent in the dispersion relation: n=1 for antiferromagnets and n=2 for ferromagnets. In order to investigate the temperature dependence of the magnetic heat capacities of the sample B below T_{c1}, we fitted the following equation to the C_{mag} data of the sample B between 1.3 and 4 K

$$C_{mag}=aT^{\alpha}+bT^{-2} \tag{3}$$

where the second term represents the high-temperature heat capacity tail of the magnetic phase transition at T_{c2} [21]. We thus got α=3.01≈3/1, a=7.49·10^{-2} J K^{-4} mol^{-1}, and b=0.982 J K mol^{-1}. The obtained spin wave heat capacity is drawn by a solid curve in Fig. 3a. On the other hand, the temperature dependence of the magnetic heat capacities of the sample B below T_{c2} was obtained by fitting the following equation to the C_{mag} data of the sample B below 0.6 K

$$C_{mag}=a'T^{\alpha'} \tag{4}$$

The best fit was obtained for α'=1.08≈1/1 (or 2/2) and a'=1.74 J K^{-2} mol^{-1} (drawn by a dashed curve in Fig. 3 a).

The spin wave analytical result for the high-temperature magnetic phase transition suggests that the MnFe-sal crystal orders in a three-dimensional antiferromagnetic state below T_{c1}. This apparently seems to be inconsistent with the ferrimagnetic ordering below T_{c1} [12], because many three-dimensional ferrimagnets indicate the same $T^{3/2}$ temperature dependence for their magnetic heat capacities as that for three-dimensional ferromagnets below the magnetic phase transition temperatures [26–28]. In contrast, a theoretical analysis in our previous paper [29] suggests that the spin wave heat capacities for three-dimensional spin systems show T^3 temperature dependence when at least one interaction path among x-, y-, and z-directions possesses antiferromagnetic character. The present spin wave analytical result is consistent with this case. On the other hand, the spin wave analysis below T_{c2} suggests that the magnetic order is either one-dimensional antiferromagnetic or two-di-

mensional ferromagnetic. Since the long-range order is theoretically impossible for one- and two-dimensional Heisenberg systems, the present result does not reflect the actual magnetic situation realized in the MnFe-sal crystal. One of the reasons for this would be that the temperature region from 0.2 to 0.6 K is not low enough for reasonable application of the spin wave theory. Another reason would be that since the high-spin Mn^{3+} ion in an octahedral ligand-field symmetry is characterized by the orbital-degenerated $^5E_{2g}$ term and thus the orbital angular momentum can contribute to the magnetism, simple spin wave approximation cannot be applicable.

Acknowledgements

This work was partially supported by a Grant-in-Aid for Scientific Research on Priority Areas 'Metal-Assembled Complexes' (Area No. 401/12023229) from the Ministry of Education, Culture, Sports, Science and Technology, Japan.

References

1 D. Gatteschi, O. Kahn, J. S. Miller and F. Palacio, Eds., Magnetic Molecular Materials, NATO ASI Series E, Vol. 198, Kluwer Academic Publishers, Dordrecht 1991.
2 O. Kahn, Molecular Magnetism, Wiley-VCH, New York 1993.
3 O. Kahn, Ed., Magnetism: A Supramolecular Function, NATO ASI Series C, Vol. 484, Kluwer Academic Publishers, Dordrecht 1996.
4 E. Coronado, P. Delhaès, D. Gatteschi and J. S. Miller, Eds., Molecular Magnetism: From Molecular Assemblies to the Devices, NATO ASI Series E, Vol. 321, Kluwer Academic Publishers, Dordrecht 1996.
5 M. M. Turnbull, T. Sugimoto and L. K. Thompson, Eds, Molecule-Based Magnetic Materials: Theory, Techniques, and Applications, ACS Symposium Series, Vol. 644, American Chemical Society, Washington, DC 1996.
6 P. M. Lahti, Ed., Magnetic Properties of Organic Materials, Marcel Dekker, New York 1999.
7 K. Ito and M. Kinoshita, Eds., Molecular Magnetism: New Magnetic Materials, Kodansha and Gordon and Breach Science Publishers, Tokyo and Amsterdam 2000.
8 H. Miyasaka, N. Matsumoto, H. Ōkawa, N. Re, E. Gallo, and C. Floriani, J. Am. Chem. Soc., 118 (1996) 981.
9 H. Miyasaka, N. Matsumoto, N. Re, E. Gallo and C. Floriani, Inorg. Chem., 36 (1997) 670.
10 M. Ohba and H. Ōkawa, Coord. Chem. Rev., 198 (2000) 313.
11 A. Bhattacharjee, Y. Miyazaki, Y. Nakazawa, S. Koner, S. Iijima and M. Sorai, Physica B, 305 (2001) 56.
12 H. Miyasaka, H. Ieda, N. Matsumoto, K. Sugiura and M. Yamashita, Inorg. Chem., 42 (2003) 3509.
13 L. J. de Jongh and A. R. Miedema, Adv. Phys., 23 (1974) 1.
14 R. L. Carlin, Magnetochemistry, Springer-Verlag, Berlin 1986.
15 M. Sorai and D. N. Hendrickson, Pure Appl. Chem., 63 (1991) 1503.
16 M. Sorai, in Molecule-Based Magnetic Materials: Theory, Techniques, and Application, M. M. Turnbull, T. Sugimoto and L. K. Thompson, Eds., ACS Symposium Series 644, American Chemical Society, Washington, DC 1996, pp. 99–114.
17 M. Sorai, Bull. Chem. Soc. Jpn., 74 (2001) 2223.
18 S. Murakawa, T. Wakamatsu, M. Nakano, M. Sorai and H. Suga, J. Chem. Thermodyn., 19 (1987) 1275.
19 Y. Kume, Y. Miyazaki, T. Matsuo and H. Suga, J. Phys. Chem. Solids, 53 (1992) 1297.
20 Y. Miyazaki, Q. Wang, Q. Yu, T. Matsumoto, H. Miyasaka, N. Matsumoto and M. Sorai, Thermochim. Acta, 431 (2005) 133.
21 H. M. J. Blöte, Physica B, 79 (1975) 427.
22 G. S. Rushbrooke and P. J. Wood, Mol. Phys., 1 (1958) 257.
23 R. L. Stephenson, K. Pirnie, P. J. Wood and J. Eve, Phys. Lett., 27A (1968) 2.
24 K. Yamaji and J. Kondo, J. Phys. Soc. Jpn., 35 (1973) 25.
25 K. Asano, K. Inoue, M. Nakano, Y. Miyazaki, M. Sorai, K. Nakatani and O. Kahn, Bull. Chem. Soc. Jpn., 72 (1999) 1749.
26 K. Asano, Y. Miyazaki, W. Mori, K. Nakatani, O. Kahn and M. Sorai, Bull. Chem. Soc. Jpn., 73 (2000) 885.
27 J. E. Kunzler, L. R. Walker and J. K. Galt, Phys. Rev., 119 (1960) 1609.
28 S. R. Pollack and K. R. Atkins, Phys. Rev., 125 (1962) 1248.
29 N. Ohmae, A. Kajiwara, Y. Miyazaki, M. Kamachi and M. Sorai, Thermochim. Acta, 267 (1995) 435.